ORNL/SPR-2022/2652

One Dimensional Penstock Flow Models for Hydropower Digital Twin

William Gurecky
Hong Wang
Shawn Ou

Approved for public release.
Distribution is unlimited.

October 2022

OAK RIDGE National Laboratory

ORNL IS MANAGED BY UT-BATTELLE LLC FOR THE US DEPARTMENT OF ENERGY

ORNL/SPR-2022/2652

Buildings and Transportation Science Division

ONE DIMENSIONAL PENSTOCK FLOW MODELS FOR HYDROPOWER DIGITAL TWIN

William Gurecky
Hong Wang
Shawn Ou

October 2022

Prepared by
OAK RIDGE NATIONAL LABORATORY
Oak Ridge, TN 37831
managed by
UT-Battelle LLC
for the
US DEPARTMENT OF ENERGY
under contract DE-AC05-00OR22725

CONTENTS

LIST OF FIGURES

LIST OF TABLES

ABBREVIATIONS

1D	one dimensional
3D	three dimensional
CFD	computational fluid dynamics
DT	digital twin

ABSTRACT

This report details the inelastic, unsteady, one-dimensional flow equations that are used to model flow through a penstock in a hydropower facility. The flow model is coupled to a mechanistic turbine model to compute the rotation rate of the turbine, which is dependent on the flow rate, gravitational head, and various parameters of the machine, such as inlet vane angle. Results are given for an example hydropower facility in which the turbine is subjected to a specified time-varying load, and the results on the flow rate are shown. Future applications for the flow model are also briefly reviewed.

1. INTRODUCTION

The elements of the hydropower facility relevant to this report are shown in figure 1. This work is primarily concerned with predicting the time-dependent mass flow rate of water through the penstock and turbine given design details of the facility, such as reservoir height, pipe diameters and lengths, and various design parameters of the turbine. This report also includes a mechanistic dynamic model of the turbine to predict its rotational speed. Additionally, calculation of the static pressure profile along the penstock as a function of time is also desired to determine forces acting on joints of the penstock walls.

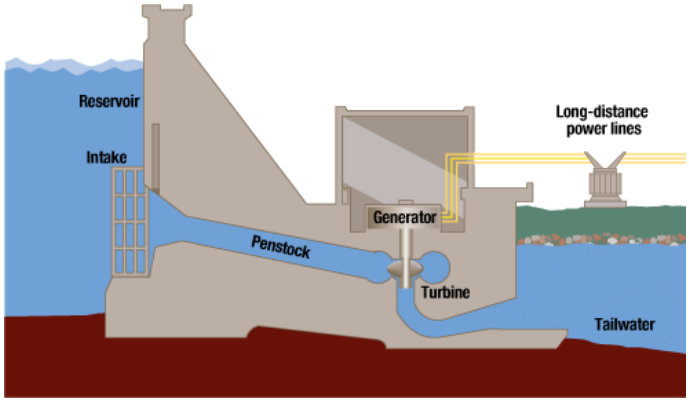

Figure 1. Simplified depiction of a hydropower facility (TVA).

This work represents the first stage of development of a larger digital twin (DT) model of the entire hydropower facility. The unsteady flow models developed herein are to be coupled to other dynamic system models of the generator, feedback control, and other electrical systems. The overarching goal of the fully coupled DT model of the hydropower facility is to accurately simulate all physics governing the hydroelectric plant operation and to incorporate all relevant experimental plant data to calibrate the models, both up-front and on-line. The tool will aid in identifying when corrective actions must be performed to maintain optimal plant operation, and it will support the design of new facilities.

1.1 FUTURE APPLICATIONS

It is envisioned that the models used in the DT, including the flow models developed in this work, will be calibrated to any particular facility by rigorous Bayesian methods given high-fidelity 3D computational fluid dynamics (CFD) simulations and experimental data, as well as by dynamically adjusting DT model parameters given real-time plant data through on-line Bayesian methods, such as particle filtering methods.

Through these adaptation procedures, the DT model will be a predictive tool for a wide variety of hydropower systems that can inform operating engineers of potential issues before they impact operations at the plant. One use case could be monitoring the dynamic stresses on the penstock walls caused by the pressure exerted by flow and water hammer. A DT model can quickly simulate a large series of “what if" scenarios that can help identify mitigation strategies. Additionally, the DT model could be used in the design of new hydropower facilities, as it will be capable of estimating the performance of the system before construction.

2. GOVERNING FLOW EQUATIONS

In this work, the unsteady flow is modeled in 1D—along the centerline of the penstock—and the flow is assumed to be inelastic. Additional elasticity of the penstock walls is also ignored. This results in a simplified constant water density model that is best applied to hydropower systems with low to moderate gravitational head, where changes in density are not as pronounced over the penstock length compared to high gravitational head scenarios. Future work will focus on the development of an elastic flow model to ensure applicability of the model to a wider variety of hydropower facilities.

The coordinate along the penstock centerline is denoted by the variable s. Consider an infinitesimal volume $\delta V = \delta s \delta n \delta y$ of fluid traveling through the penstock, confined to travel on a streamline following the centerline of the penstock. The dimension of the infinitesimal volume pointed along the direction of the penstock is δs, and the area of the infinitesimal volume orthogonal to the flow direction s is $\delta A = \delta n \delta y$. Figure 2 depicts a front view of the infinitesimal fluid volume, with the dimension y into the page.

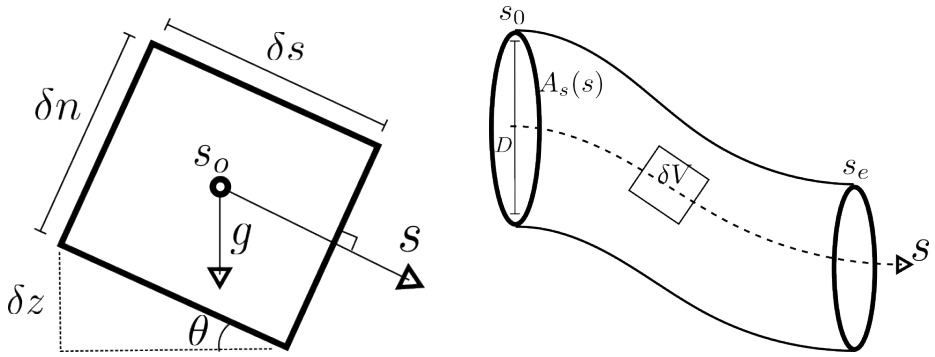

(a) Infinitesimal fluid volume element, δV.

(b) Infinitesimal volume flowing along centerline of penstock.

Figure 2. Differential analysis of flow of along the penstock centerline.

A variety of forces are acting upon this fluid volume, including pressure on the front and rear faces, viscous friction forces from the walls, gravitational forces, and inertial forces from the flow. Applying Newton’s second law to the fluid volume results in

$$\sum F = \rho \delta V a_s, \tag{1}$$

where ρ is the water density and is constant. a_s is the acceleration of the fluid volume along the s direction. We can write the acceleration as the time derivative of the velocity along the penstock centerline: $a_s = \frac{\partial v_s}{\partial t}$. The velocity is a function of location and time, $v_s = v_s(s(t), t)$, so the time derivative in total can be written using the chain rule as follows:

$$a_s = \frac{Dv_s}{Dt} = \frac{\partial v_s}{\partial t}\frac{\partial t}{\partial t} + \frac{\partial v_s}{\partial s}\frac{\partial s}{\partial t} \tag{2}$$

From a Lagrangian perspective, the position of the infinitesimal fluid volume changes with time $\frac{\partial s}{\partial t} = v_s$, so

$$a_s = \frac{\partial v_s}{\partial t} + v_s\frac{\partial v_s}{\partial s}. \tag{3}$$

Rewriting Eq. (1) yields

$$\frac{1}{\rho\delta V}\sum F = \frac{\partial v_s}{\partial t} + v_s\frac{\partial v_s}{\partial s}. \tag{4}$$

Next, all the relevant forces acting on the infinitesimal fluid volume are summed.

The force due to gravity is as folllows:

$$\begin{aligned} F_g &= (s \cdot g)\rho\delta V \\ &= \sin(\theta)g\rho\delta V \\ &= \frac{\delta z}{\delta s}g\rho\delta V, \end{aligned} \tag{5}$$

where θ is the angle of the pipe, and g is the gravitational constant, which is a vector pointing down.

The net force on the fluid volume due to pressure acting on the front and rear faces is

$$F_p = \delta n\delta y\left(p_{s_o-\delta s/2} - p_{s_o+\delta s/2}\right). \tag{6}$$

Let $\delta p = p_{s_o-\delta s/2} - p_{s_o+\delta s/2}$. Summing all the forces, Eq. (4) becomes

$$\frac{1}{\delta V}\left[F_p + F_g\right] = \rho\frac{\partial v_s}{\partial t} + \rho v_s\frac{\partial v_s}{\partial s} \tag{7}$$

$$\frac{1}{\delta s\delta n\delta y}\left[\delta n\delta y\delta p + \rho g\frac{\delta z}{\delta s}\delta s\delta n\delta y\right] = \rho\frac{\partial v_s}{\partial t} + \rho v_s\frac{\partial v_s}{\partial s}.$$

Letting the element size approach zero, $\delta s \to 0$ and $\delta z \to 0$:

$$-\frac{\partial p}{\partial s} + \rho g\frac{\partial z}{\partial s} = \rho\frac{\partial v_s}{\partial t} + \rho v_s\frac{\partial v_s}{\partial s}. \tag{8}$$

The velocity of the flow in the penstock is related to the mass flow rate, q, by:

$$v_s = \frac{q}{\rho A_s}. \tag{9}$$

$A_s = A_s(s)$ represents the flow area of the penstock and may be a function of distance down the penstock. Assuming the density remains constant, and assuming the velocity v_s is uniform over a cross sectional area

of the penstock and represents the flow area–averaged velocity, Eq. (1) can be written in terms of mass flow rate by substituting Eq. (9) into Eq. (8), resulting in

$$-\frac{\partial p}{\partial s} + \rho g \sin(\theta) = \rho \frac{\partial(\frac{q}{\rho A_s})}{\partial t} + \rho(\frac{q}{\rho A_s})\frac{\partial(\frac{q}{\rho A_s})}{\partial s}, \tag{10}$$

and since the density is constant,

$$-\frac{\partial p}{\partial s} + \rho g \sin(\theta) = \frac{\partial(\frac{q}{A_s})}{\partial t} + \frac{q}{\rho A_s}\frac{\partial(\frac{q}{A_s})}{\partial s}. \tag{11}$$

Since A_s is a function of s, it remains under the differentiation operator in the last term; however, the mass flow rate is not a function of s in the penstock by the conservation of mass and from the incompressible assumption; thus,

$$-\frac{\partial p}{\partial s} + \rho g \frac{\partial z}{\partial s} = \frac{1}{A_s}\frac{\partial q}{\partial t} + \frac{q^2}{\rho A_s}\frac{\partial(\frac{1}{A_s})}{\partial s}. \tag{12}$$

Note that in this formulation each term in this differential equation describes a contribution to the pressure change per unit length, each having units of [Pa/m].

2.1 WALL FRICTION

The impact of friction can be incorporated into the flow model by first considering the pressure loss due to friction. One can estimate this loss by the Darcy–Weisbach relationship (Muson et al. [2009]):

$$\delta p_f = (\rho g) f \frac{\delta s}{D}\frac{v_s^2}{2g}, \tag{13}$$

where D is the pipe diameter and, assuming the flow is fully developed, f is the friction factor is given by the Colebrook formula:

$$\frac{1}{\sqrt{f}} = -2\log\left(\frac{\epsilon/D}{3.7} + \frac{2.51}{\mathrm{Re}\sqrt{f}}\right), \tag{14}$$

which is a transcendental equation that can be solved using fixed-point iteration to obtain f given the pipe roughness, ϵ, and diameter D. The pressure drop per unit length is

$$\frac{\delta p_f}{\delta s} = (\rho g)\frac{f}{D}\frac{v_s^2}{2g}, \tag{15}$$

and substituting $v_s = q/(\rho A_s)$,

$$\frac{\delta p_f}{\delta s} = (\rho g)\frac{f}{D}\frac{(q/(\rho A_s))^2}{2g} = \frac{f q^2}{2D\rho A_s^2}. \tag{16}$$

Let $c_f = \frac{f}{2D\rho}$. The time-dependent mass flow rate may be updated as

$$-\frac{\partial p}{\partial s} - c_f\frac{q^2}{A_s^2} + \rho g\frac{\partial z}{\partial s} = \frac{1}{A_s}\frac{\partial q}{\partial t} + \frac{q^2}{\rho A_s}\frac{\partial(\frac{1}{A_s})}{\partial s}. \tag{17}$$

2.2 INTEGRATION ALONG THE PENSTOCK

This partial differential equation can be integrated along the penstock length, giving

$$\int_{s_0}^{s_e} \left[-\frac{\partial p}{\partial s} - c_f \frac{q^2}{A_s^2} + \rho g \frac{\partial z}{\partial s} \right] ds = \int_{s_0}^{s_e} \left[\frac{1}{A_s} \frac{\partial q}{\partial t} + \frac{q^2}{\rho A_s} \frac{\partial (\frac{1}{A_s})}{\partial s} \right] ds, \tag{18}$$

where s_0 is the inlet and s_e is the outlet location and are the limits of integration.

$$-p_e(t) + p_0(t) - q^2 I_{A_2} + \rho g(z_e - z_0) = \frac{\partial q}{\partial t} I_{A_1} + \frac{q^2}{2\rho} \left(\frac{1}{A_e^2} - \frac{1}{A_0^2} \right), \tag{19}$$

where $p_e = 0$ (zero gauge pressure at the outlet) and p_0 are known, and A_e and A_0 are the outlet and inlet area, respectively, and

$$I_{A_1} = \int_{s_0}^{s_e} \left[\frac{1}{A_s} \right] ds \tag{20}$$

$$I_{A_2} = \int_{s_0}^{s_e} \left[\frac{c_f}{A_s^2} \right] ds. \tag{21}$$

In the software implementation, both integrals are estimated using the trapezoidal rule along each pipe segment in the penstock.

After integration, we are left with an ordinary differential equation governing the time-dependent mass flow rate through the penstock.

$$\boxed{\frac{dq}{dt} = \frac{1}{I_{A_1}} \left[-p_e(t) + p_0(t) - q^2 I_{A_2} + \rho g(z_e - z_0) - \frac{q^2}{2\rho} \left(\frac{1}{A_e^2} - \frac{1}{A_0^2} \right) \right]} \tag{22}$$

This form neglects the presence of a turbine, but Section 3. discusses the coupling of this equation with a turbine model to form a complete description of the hydropower fluid system. Effectively, an additional pressure loss term from the turbine will be included in the governing flow equation.

2.3 INCLUDING VALVE AND OTHER LOSSES

The prior derivation of the mass flow rate neglected the inclusion of losses through valves, bends, and the turbine. These losses are treated similarly to the friction pressure loss, δp_f, in equation 13, but the math models of a valve or turbine pressure loss are significantly different. Additionally, valve losses are assumed to be applied at a single point. The valve internals are not explicitly modeled.

For a valve, the pressure loss across a valve can be computed by

$$\Delta p_L = K_L \frac{\rho v_s^2}{2}, \tag{23}$$

where K_L is the valve loss coefficient and is a function of the valve open fraction and the internal geometry of the valve. This valve pressure loss Δp_L can be easily added as a new term to Eq. (22). Pipe bend as well as entrance and exit losses can be handled in a similar manner.

2.4 PRESSURE PROFILE FOR INCOMPRESSIBLE UNSTEADY FLOW

The pressure can be computed by sweeping through the penstock from the outlet, where the known pressure boundary condition of 0 gauge pressure is specified, back to the penstock inlet. Given that the mass flow rate in the system does not change as a function of s due to conservation of mass and from the incompressibility assumption, the pressure balance on each segment of pipe can be derived from Eq. (17). Instead of integrating this equation over the entire penstock domain, the integration can be performed in steps from segment to segment. Starting from the outlet at s_e to the next upstream pipe joint s_{e-1}, the integration yields

$$\int_{s_{e-1}}^{s_e} \left[-\frac{\partial p}{\partial s} - c_f \frac{q^2}{A_s^2} + \rho g \frac{\partial z}{\partial s} \right] ds = \int_{s_{e-1}}^{s_e} \left[\frac{1}{A_s} \frac{\partial q}{\partial t} + \frac{q^2}{\rho A_s} \frac{\partial (\frac{1}{A_s})}{\partial s} \right] ds, \tag{24}$$

where $\dot{q} = \frac{dq}{dt}$ is known from the solution of Eq. (22). Isolating the pressure terms on the left-hand side, we obtain

$$-p_e + p_{e-1} = b_{e-1} \tag{25}$$

with

$$b_{e-1} = -I_{A_1} \dot{q} - q^2 I_{A_2} + \rho g (z_e - z_{e-1}) - \frac{q^2}{2\rho} \left(\frac{1}{A_e^2} - \frac{1}{A_{e-1}^2} \right). \tag{26}$$

We note that $p_e = 0$ by definition, since the outlet is always open to the atmosphere, so the static pressure here is known. By marching from the outlet back toward the inlet, a linear system of equations can be constructed of the following form:

$$\begin{bmatrix} 1 & -1 & 0 & 0 & 0 \\ 0 & 1 & -1 & 0 & 0 \\ 0 & 0 & 1 & -1 & 0 \\ 0 & 0 & 0 & 1 & -1 \\ 0 & 0 & 0 & 0 & 1 \end{bmatrix} \begin{bmatrix} p_{e-4} \\ p_{e-3} \\ p_{e-2} \\ p_{e-1} \\ p_e \end{bmatrix} = \begin{bmatrix} b_{e-4} \\ b_{e-3} \\ b_{e-2} \\ b_{e-1} \\ 0 \end{bmatrix}. \tag{27}$$

The pressure profile $[p_{e-N}, ...p_e]$, can be obtained by solving Eq. (27) using Gaussian elimination.

3. TURBINE DYNAMIC MODEL

The Francis turbine design is the focus of the present work. A visual representation of a Francis turbine is given in Figure 3.

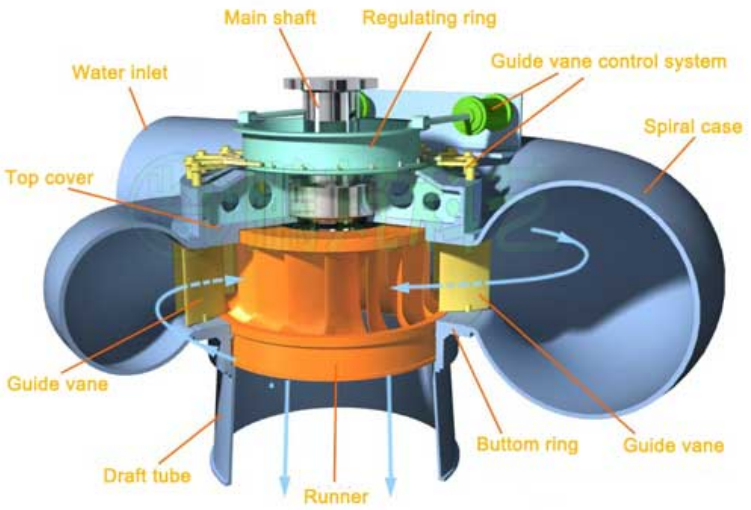

Figure 3. A Francis turbine with key components shown (Vytvytskyi and Lie [2018]).

Here, we consider the inlet guide vane angle to be a controllable parameter; in the full DT model, this would be under closed loop control such that the vane angle is adjusted to maintain the appropriate rotation rate. Other important aspects of the Francis turbine considered in the following models are the outer radius of the runner, inner runner radius and the height, and angles of the runner blades.

3.1 TORQUE BALANCE

First, a torque balance is written for the turbine runner, shaft, and generator rotor. The moment of inertia of all these spinning components is denoted as J. Torques applied to the shaft are the following: (1) torque applied by the fluid on the runner vanes as the vanes deflect the flow, T_w, (2) torque applied by bearings from friction losses, T_B, and (3) torque from the generator load, T_L.

$$J\frac{d\omega}{dt} = T_w - T_L - T_B. \tag{28}$$

This ordinary differential equation (ODE) is coupled to the flow equation through the T_w term, as the torque applied by the flow moving through the turbine depends on the flow rate, among other things. Equation (28) and Eq. (22) form a coupled system of ODEs that can be stepped forward together using a suitable time integration scheme, such as the popular Runge–Kutta methods.

The load torque, T_L, is assumed to be a known quantity in this report, and it may be a function of time. In reality, the load torque depends on the generator model and grid load. A complete load model and coupling to the power grid is beyond the scope of this report. The friction torque is assumed to follow the simple linear relationship $T_B = b\omega$, where b is a constant and is set to 1, but it could be tuned provided data. The flow torque, T_w, is the most complex term in the torque balance and is computed using conservation of mass and momentum of the flow through the turbine. This torque is reviewed in the following section.

3.2 TURBINE FLOW MODEL

The turbine model developed by Vytvytskyi and Lie [2018] is adopted in this work and is briefly reviewed here. This model relates the flow rate q, vane angle α_1, and rotation rate ω to shaft torque, T_w, produced by the flow of water through the turbine. Furthermore, this model includes a variety of loss terms in the pressure loss formulation, including the effects of friction, shock, and whirl. The model contains several tunable parameters that could be obtained via CFD modeling or by experiment.

From the model developed by Vytvytskyi and Lie [2018], the shaft power generated by the flow through the turbine is given by

$$\dot{W}_s = q\omega\left(R_1\frac{\dot{V}}{A_1}\cot(\alpha_1) - R_2\left[\omega R_2 + (\dot{V}/A_2)\cot\beta_2\right]\right), \tag{29}$$

where $\dot{V} = q/\rho$ is the volumetric flow rate, α_1 is the inlet guide vane angle, R_1 is the outer runner radius, R_2 is the inner runner radius, A_1 is the runner inlet flow area, and A_2 is the runner outlet flow area. β_1 is the inlet blade angle, and β_2 is the outlet blade angle.

The torque supplied to the shaft due to the flow is

$$T_w = \dot{W}_s/\omega. \tag{30}$$

Equation (30) can be plugged into Eq. (28) to complete the torque balance.

The energy loss due to friction is given by

$$\dot{W}_{ft} = k_{ft,1}\dot{V}(\cot\gamma_1 - \cot\beta_1)^2 + k_{ft,2}\dot{V}\cot^2\alpha_2 + k_{ft,3}\dot{V}^2, \tag{31}$$

where $k_{ft,1}$, $k_{ft,2}$, and $k_{ft,3}$ are tunable loss coefficients representing the shock, whirl, and flow friction losses through the turbine, respectively. These coefficients can be determined by Bayesian inference using data collected via experimental means, or by executing a series of high-fidelity CFD simulations of the turbine. α_2 may be computed from $\cot(\alpha_2) = \cot(\beta_2) + \omega R_2/(\dot{V}/A_2)$ and $\cot(\gamma_1) = \cot(\alpha_1) - \omega R_1 A_1/\dot{V}$.

The net work rate done by the water on the turbine is

$$\dot{W}_t = \dot{W}_s + \dot{W}_{ft}, \tag{32}$$

but only $\dot{W}_s$ is usable work with $\dot{W}_{ft}$ representing losses and inefficiency in the system. The turbine efficiency may be defined as

$$\eta = \frac{\dot{W}_s}{\dot{W}_t}. \tag{33}$$

4. RESULTS

4.1 PENSTOCK WITH SINGLE VALVE AND NO TURBINE

First, the 1D flow model was applied to simplified penstock without a coupled turbine model. This case models an 80 m reservoir discharging through a penstock with a controllable sluice gate valve. The flow rate through the system may be controlled by opening and closing the valve, which impacts the valve's loss coefficient, K_L, given in Eq. (23). The parameters of the penstock model are given by Table 1.

Table 1. Penstock parameters.

Parameter	Value	Unit
Penstock diameter, D	1.0	[m]
Penstock length	148	[m]
Gravitational head, z_h	80	[m]
Wall roughness, ϵ	1E-5	[m]

Figure 4 shows the geometry of the pipe and valve for this case. The penstock in this example case is horizontal, starting from the base of the reservoir and discharging at the same height. The reservoir height is 80 m. The loss coefficient of the sluice gate is computed according to K_L = 1E-3 +0.8(1E-2+1/$a^{1.3}$), where $a \in (0, 1]$ is the valve open fraction.

The inlet valve is initially closed and allowed to gradually open at an opening fraction rate of $0.05/s$, such that the gate requires 20 s to completely open. The initial mass flow rate is 0 kg/s. At 60 s, the valve is closed to the 60% open position. Figure 5 shows the volumetric flow rate through the penstock as the valve is opened initially and then partially closed. Figure 7 shows the static gauge pressure profile in the pipe in atmospheres at the end of the simulation, t =160 s. The valve open fraction vs. time is plotted in Figure 6.

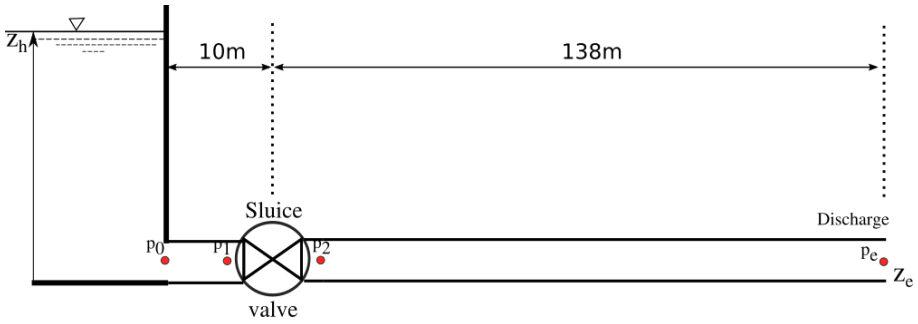

Figure 4. Penstock model with valve only and no slope.

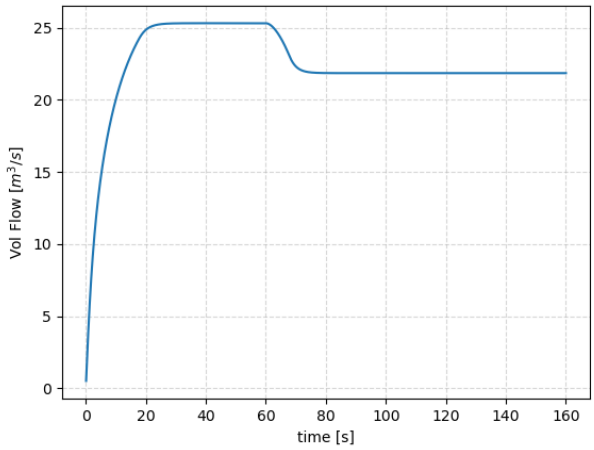

Figure 5. Volumetric flow rate vs. time.

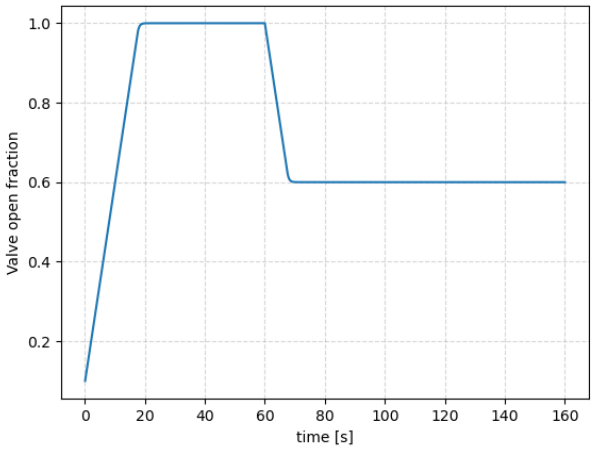

Figure 6. Sluice valve open fraction vs. time.

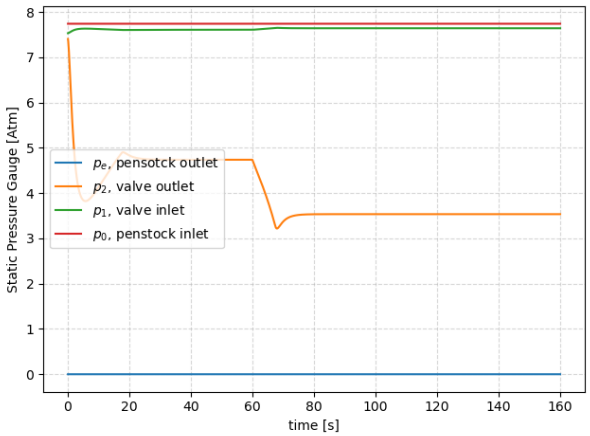

Figure 7. Static gauge pressure vs. time at each pressure tap location.

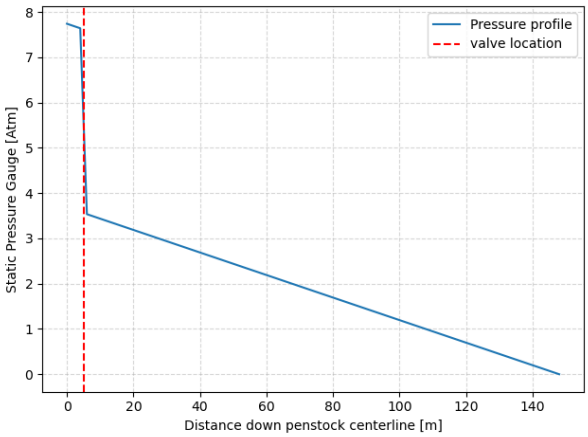

Figure 8. Static gauge pressure profile along the penstock at t =160 s.

4.2 PENSTOCK WITH TURBINE MODEL

For this demonstration of the coupled flow and turbine model, we consider the turbine inlet vane angle, α_1, to be under open loop control. In future work, the inlet guide vane angle will be under closed loop control using a proportional, integral, differential control scheme so as to maintain a set rotation rate. The parameters of the coupled turbine and penstock model are given by Table 2.

Table 2. Turbine and penstock parameters.

Parameter	Value	Unit
Penstock diameter	1.0	[m]
Penstock length	148	[m]
Reservoir height, z_h	80	[m]
z_0	50	[m]
z_e	0	[m]
J	10,000	[kg m^2]
R_1	1.01	[m]
R_2	0.737	[m]
β_1	111.0	[deg]
β_2	162.5	[deg]
$k_{ft,1}$	1E5	—
$k_{ft,2}$	1E1	—
$k_{ft,3}$	4E3	—

The penstock geometry and pressure tap locations are shown in Figure 9. The static pressure is recorded at each tap location and is plotted as a function of time in the following sections in Figures 15 and 23. Accurate computation of the static pressure profile in the penstock is important for studying the stresses on the penstock walls. Some extreme scenarios, such as a sudden large blockage near the intake of the penstock, could potentially lead to vacuum conditions in some portions of the penstock, and it is important for the model to accurately capture these effects.

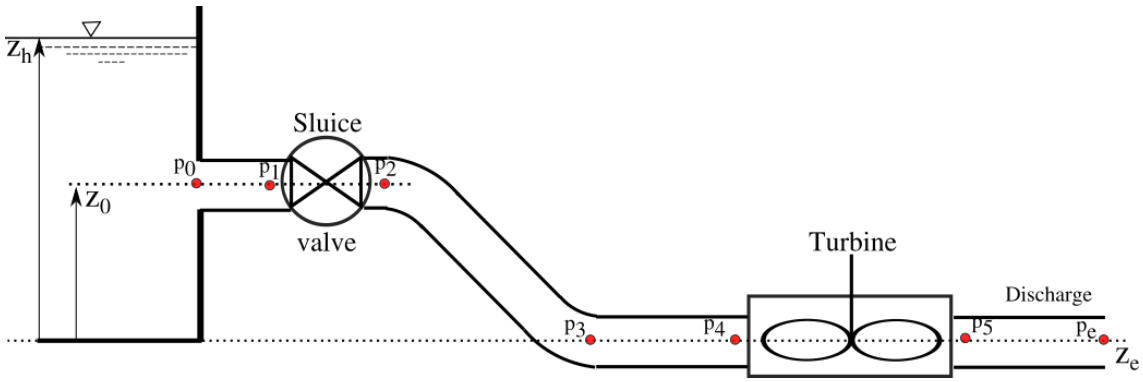

Figure 9. Penstock geometry with valve and turbine.

4.2.1 Startup Transient

In the following simulations, the turbine starts from rest with $\omega = 0$. The inlet sluice gate is initially closed and allowed to gradually open at an opening fraction rate of $0.05/s$, such that the gate requires 20 s to completely open. The turbine inlet guide vane angle is set to $\alpha_1 = \pi/8$. Additionally, a ramped load torque is imposed on the turbine to prevent high rotation rates, or a runaway condition, during startup. The increase in flow spins the turbine up to a steady-state rotation rate at which the torque produced by the flow balances the imposed load torque. After this steady-state flow and rotation rate are met, Case 1 and Case 2 simulations are started.

4.2.2 Case 1: Load Torque Perturbations

After the coupled system is allowed to come to equilibrium flow and rotation rate conditions after approximately 60 s, the turbine is subjected to small 10% changes to the load torque, T_L. In reality, this load would arise from the generator coupled to the electric grid; however, in this example, the load is a known function of time.

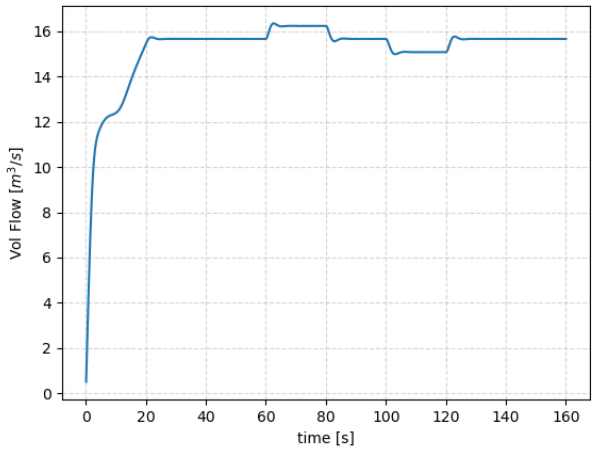

Figure 10. Volumetric flow rate vs. time.

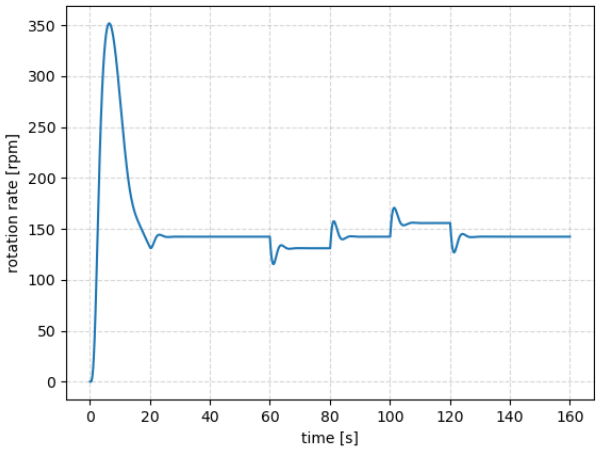

Figure 11. Turbine rotation rate vs. time.

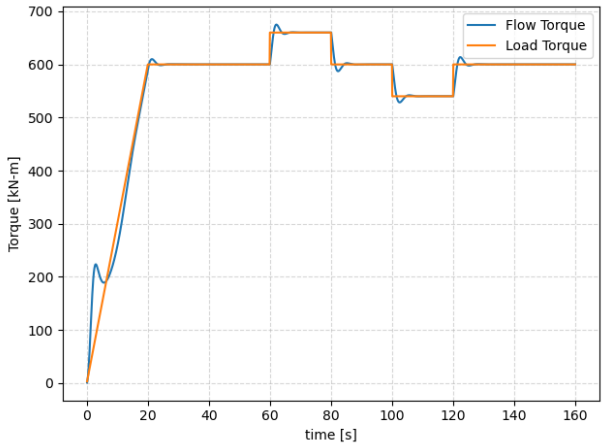

Figure 12. Turbine torque vs. time.

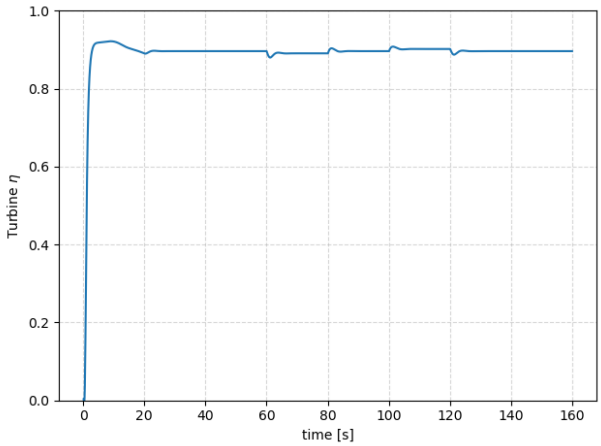

Figure 13. Turbine efficiency vs. time.

The results show that an increase in the applied load torque at t=60 s gives an expected decrease in the turbine rotation rate, as shown in Figure 11. In order to achieve torque balance, shown in figure 12, and thus achieve a steady rotation rate, the flow torque must increase to balance the increased load torque. The inverse is true when decreasing the load torque from nominal conditions at t=100 s.

Note the increase in the static pressure as the water traverses down the penstock in Figures 15 and 16. These figures show the pressures at the tap locations given in Figure 9 as a function of time and space, respectively. Figure 16 is generated at t=160 s, when the system is at steady state. This rise in static pressure as the flow traverses down the penstock occurs as gravitational head is exchanged for static pressure and because there is a large flow restriction imposed by the turbine. When the flow is in steady state, Bernoulli's principle holds, where $C = p + \rho g z + (1/2)\rho v^2 + \Delta p_{loss}$ is constant along a streamline—and since the area A_s is constant, by mass conservation, v is constant. In the penstock geometry used in this example, the 50 m drop in z over the penstock length is accompanied by a rise in static pressure, p, leading up to the turbine inlet. Consider three static pressure tap points: point (1) at the outlet of the sluice gate at the top of the penstock, point (2) at the turbine inlet and point (3) at the penstock outlet where $p_3 \approx 0$. If the flow area is constant, and ignoring friction losses and only including the turbine loss: $p_1 + \rho g z_1 = p_2 + \rho g z_2 = p_3 + \rho g z_3 + \Delta p_{loss}$. Since $z_1 >> z_2$ and $z_2 = z_3 = 0$, for sufficiently large Δp_{loss}; $p_2 > p_1$.

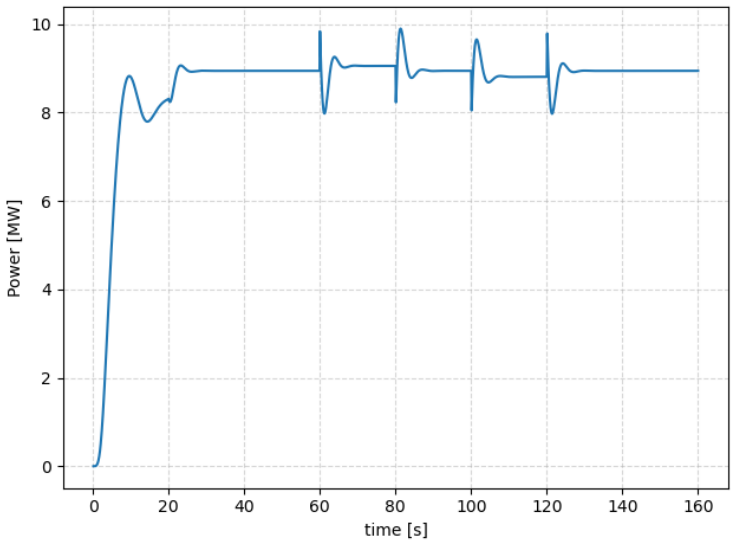

Figure 14. Turbine shaft power vs. time.

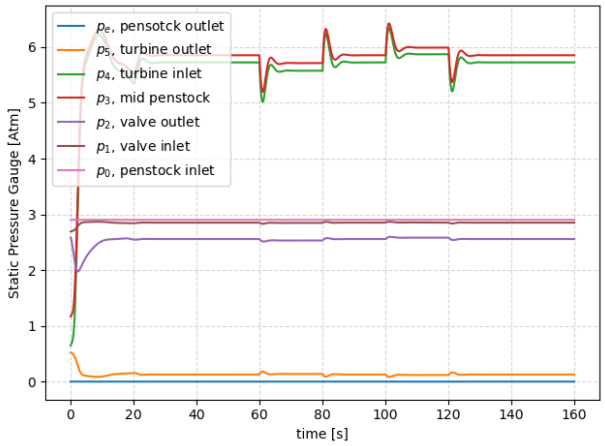

Figure 15. Gauge static pressure at different locations along the penstock vs. time.

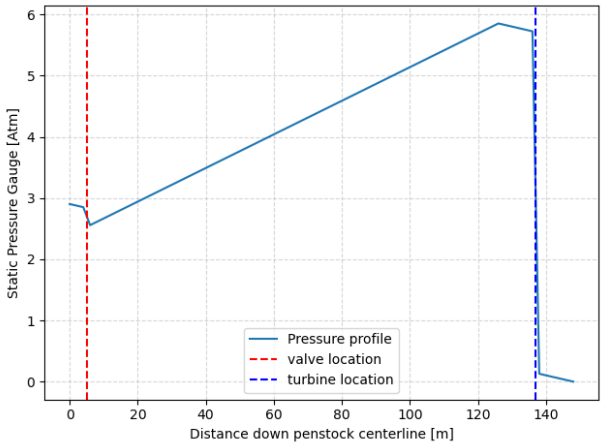

Figure 16. Static gauge pressure along the penstock at t =160 s.

4.2.3 Case 2: Inlet Guide Vane Perturbations

In this case, the inlet guide vane angle was opened from $\alpha_1 = \pi/8$ to $\alpha_1 = \pi/4$ at t=60s, then was closed back to $\pi/8$ at 80s. Then, at 100s, the guide vane is closed to $\pi/12$ and finally at t=120s is set back to $\pi/8$. The vane angle is plotted as a function of time in Figure 22. In the dynamic model, the rate at which the guide vanes move is fixed to 0.1 radians per second. Seen in figure 19, the load torque was held constant at 600 [kN-m] and in this case the sluice valve remained completely open.

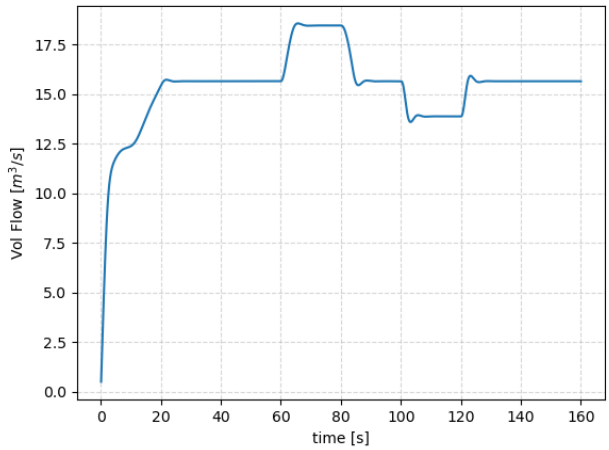

Figure 17. Volumetric flow rate vs. time.

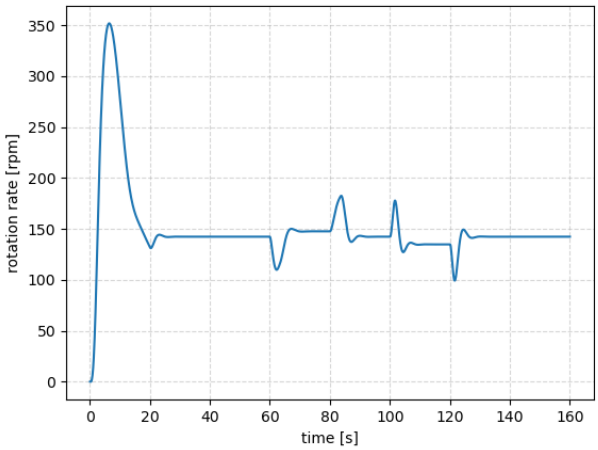

Figure 18. Turbine rotation rate vs. time.

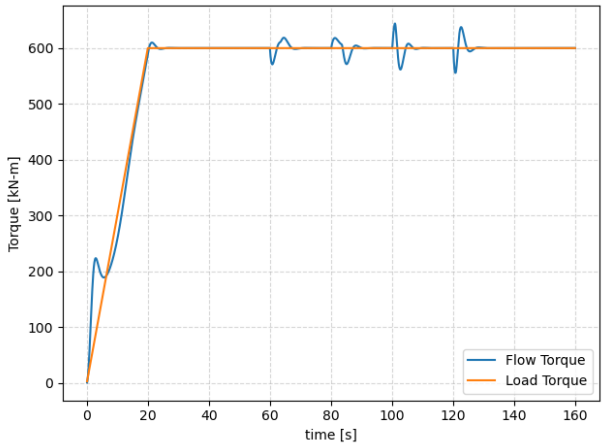

Figure 19. Turbine torque vs. time.

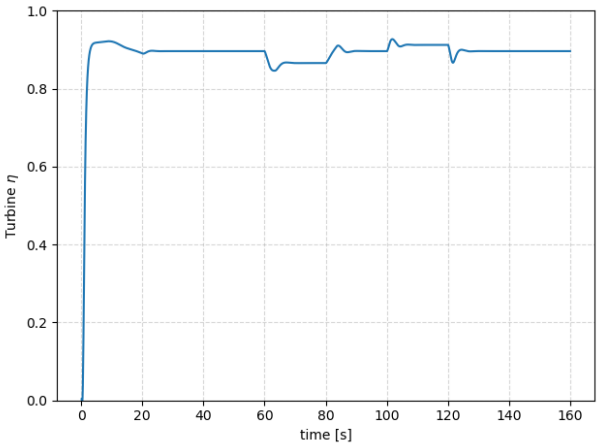

Figure 20. Turbine efficiency vs. time.

When the guide vane is opened at t=60 s from $\pi/8$ to $\pi/4$, Figure 17 shows the flow rate increases, and Figure 21 shows the overall power produced by the turbine increases. Interestingly, the efficiency of the turbine is diminished at this inlet vane angle, as shown in Figure 20. After reducing the vane angle to $\pi/12$ at t=100s, the inverse is true.

The static pressure drop across the turbine can be seen in Figures 23 and 24, which give the static pressure throughout the system as a function of time (Fig. 23) and space (Fig. 24). The location of the turbine is denoted by a blue dashed line.

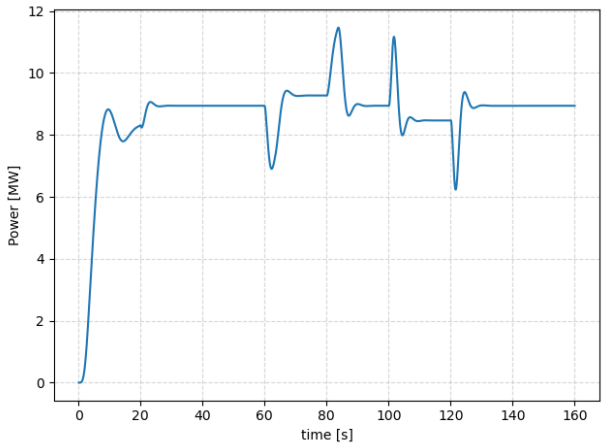

Figure 21. Turbine shaft power vs. time.

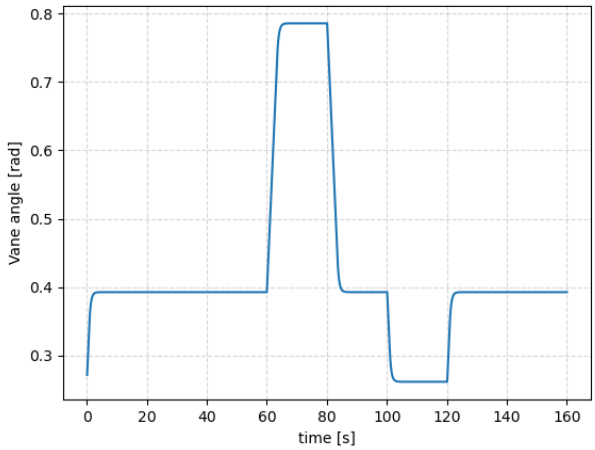

Figure 22. Inlet vane angle vs. time.

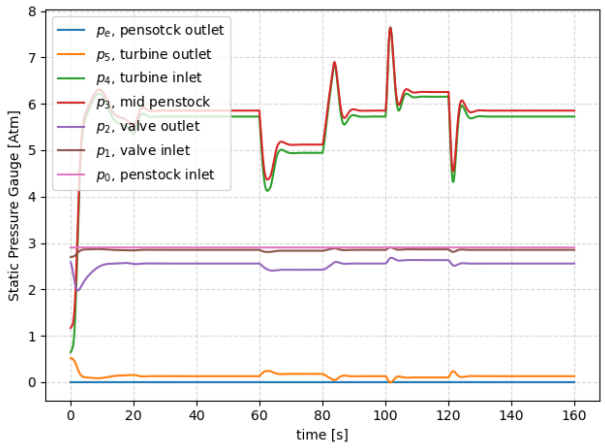

Figure 23. Gauge static pressure at different locations along the penstock vs. time.

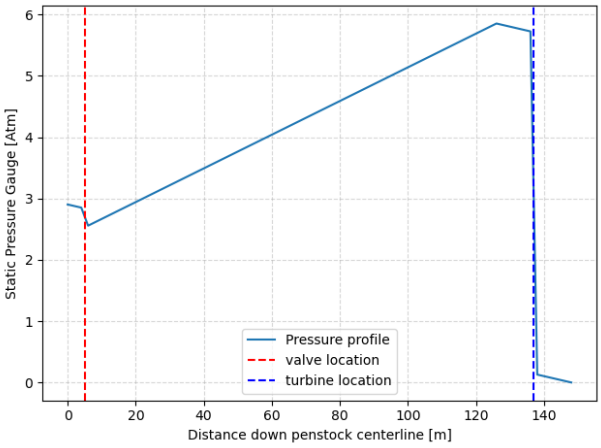

Figure 24. Static gauge pressure along the penstock at t =160 s.

5. CONCLUSION

A 1D inelastic model was developed for flow through a penstock and was coupled to a dynamic model of the turbine. The coupled model was demonstrated in an open loop control configuration in which the turbine inlet vane angles were adjusted as a function of time, and the results on the flow rate and rotation rate of the turbine were computed and visualized. This work serves as the first step toward a digital twin model of the complete hydroelectric facility. Work remains to include the effects of elasticity into the flow model and to implement a closed loop control scheme to adjust the inlet vane angle to maintain a set rotation rate. Additionally, coefficients that appear in the present model, such as the friction loss coefficients, could be tuned given experimental or CFD-born data. Furthermore, development of new turbine models including data-driven machine learning models are possible avenues for future work.

6. ACKNOWLEDGEMENTS

This work was supported by the DOE's Water Power Technologies Office and used resources at the National Transportation Research Center at Oak Ridge National Laboratory, a User Facility of DOE's Office Energy Efficiency and Renewable Energy.

7. REFERENCES

B. Muson, D. Yound, H. Okiishi, and W. Huebsch. *Fundamentals of Fluid Mechanics*. 2009.

TVA. How hydroelectric power works. URL https://www.tva.com/energy/our-power-system/hydroelectric/how-hydroelectric-power-works.

L. Vytvytskyi and B. Lie. Mechanistic model for francis turbines in openmodelica. *International Federation of Automatic Control Conference Proceedings*, 51, 2018.